Proceedings of the IASS 2024 Symposium
Redefining the Art of Structural Design
August 26-30, 2024, Zurich, Switzerland
Philippe Block, Giulia Boller, Catherine DeWolf,
Jacqueline Pauli, Walter Kaufmann (eds.)

Modelling of prestress losses in 3D tendon layout optimization using strain energy minimization

Hanna DOMNICK [*], Juan Pablo OSMAN-LETELIER [a]

[*] KLÄHNE BUNG Ingenieure
Behrenstraße 29, 10117 Berlin
hanna.domnick@gmail.com

[a] schlaich bergermann partner (sbp)

Abstract

This paper addresses the tendon layout optimization in spatial thin-walled concrete structures, building on the results achieved in [1] and [2]. Unlike previous work, which assumed a constant prestressing force along the tendon, this investigation considers prestress losses in similar structures and boundary conditions. Prestress losses are modeled as a function over the beam-like structure's length and subtracted from the initial prestressing force. Consequently, the resulting function for the prestressing force becomes dependent on the tendon layout and position along the beam-like structure. Using models for prestress losses presented in current literature, e.g. in [3], this paper outlines the calculation of these losses, the underlying assumptions, simplifications, and their practical implementation in a Matlab script. As study cases, a two-dimensional tendon layout in a beam and a three-dimensional tendon layout in a folded slab are investigated. The comprehensive approach presented in this paper provides a more accurate and realistic representation of the structural behavior in spatial prestressed concrete structures and their optimization. Thus, it enhances the understanding of the associated complexities and contributes to advancements in structural engineering and saving material through structural optimization, which is in the eyes of the authors a key component in redefining the art of structural design.

Keywords: prestressed concrete, prestress losses, thin-walled structures, tendon layout optimization

1. Introduction

In previous work, Domnick and Osman-Letelier [1] proposed a new optimization method for spatial tendon layouts based on strain energy minimization. By applying the Rayleigh-Ritz method and Lagrange multipliers, the method identifies a tendon layout in a thin-walled concrete structure that complies with practical boundary conditions and minimizes the structure's deflection. Domnick and Osman-Letelier [1] successfully optimized tendon layouts in thin-walled concrete structures with a variety of support conditions and design constraints. However, thus far, a constant prestressing force has been assumed, not taking into account prestress losses. Prestress losses reduce the prestressing force by up to 40% [3] or even 60% [4]. Hence, not considering them in the design stage can substantially weaken or even eliminate the tendon's effectiveness. Therefore, this paper extends the proposed method to the consideration of prestress losses. Considering prestress losses during the optimization enables the engineer to counteract not only the structure's deflection but also prestress losses along the tendon.

Prestress losses in post-tensioned structures occur instantly as well as over time and depend on various parameters regarding the structure's geometry and material, as well as ambient conditions and loading. There are several methods and approaches to determining those losses, ranging from rough estimations

for early design stages to more precise analytical or experimental calculations [3, 4, 5]. However, only few investigations have considered spatial tendon layouts. One notable study that investigates the estimation of friction losses for spatial tendons in a curved, prestressed bridge is by de Roeck [6].

2. Prestress Losses

The effectiveness of prestress depends heavily on the correct estimation of the prestressing force. Underestimating it can result in excessive camber and an inefficient design, while overestimating it may cause excessive deflection, resulting in unexpected cracks and a reduction of the structure's durability. The prestressing force is not constant throughout the tendon. It decreases due to geometric and material influences along the tendon and over time due to the materials' response to the applied stresses. The difference between the initial prestressing force and the resulting force in the tendon is described by the term *prestress losses*. These are grouped into instant losses and time-dependent losses. Instant losses include those due to friction, anchorage grip and elastic deformation. Time-dependent losses occur as a result of steel relaxation, concrete shrinkage as well as concrete creep.

When tensioned, the tendon is pressed against the surrounding material. The friction between tendon and surrounding material leads to a decrease in the resulting prestressing force within the tendon. These losses depend on the tendon's layout, especially the tendon's curvature, as a stronger curvature increases the friction. Losses due to elastic deformation occur due to the elastic lengthening of the tendon and shortening of the concrete. These losses depend on material parameters, e.g. their elastic moduli. Time-dependent losses due to creep, shrinkage and relaxation are mainly influenced by the timing and magnitude of the applied loads, the chemical composition of the concrete and the ambient conditions. The tendon layout has a minor influence on time-dependent losses. [3]

3. Definition of the optimization problem

The general formulation of the optimization problem is shown by Domnick and Osman-Letelier [1]. The complete constrained optimization problem for a spatial tendon layout that is described by the curve $\boldsymbol{r} : \mathbb{R} \to \mathbb{R}^3$ is defined as follows:

Minimize $\boldsymbol{r}$	$\mathcal{J}_P$	subject to	$\boldsymbol{g} = \boldsymbol{0}$	(1)
Find	$\tilde{\boldsymbol{r}} : \mathbb{R} \to \mathbb{R}^3$	with	$\lim_{n\to\infty} \tilde{\boldsymbol{r}} = \boldsymbol{r}$	(2)
by solving	$\nabla\mathcal{L} = \boldsymbol{0}$	for	$\boldsymbol{a} \in \mathbb{R}^n$	(3)
		with	$\mathcal{L}(\boldsymbol{a}) = \mathcal{J}_P(\boldsymbol{a}) + \boldsymbol{\lambda} \cdot \boldsymbol{g}(\boldsymbol{a})$	(4)
			$\mathcal{J}_P = \int_L \left(M_E(x) + M_P(\boldsymbol{a}, x)\right)^2 \, dx$	(5)
			$\tilde{\boldsymbol{r}}(\boldsymbol{a}, x) = \begin{bmatrix} \tilde{r}_x \\ \tilde{r}_y \\ \tilde{r}_z \end{bmatrix} = \begin{bmatrix} x \\ f_y\left(x, \boldsymbol{a}^T\boldsymbol{\phi}(x)\right) \\ f_z\left(x, \boldsymbol{a}^T\boldsymbol{\phi}(x)\right) \end{bmatrix}$	(6)
			$\phi_i(x) = x^{i-1}$	(7)

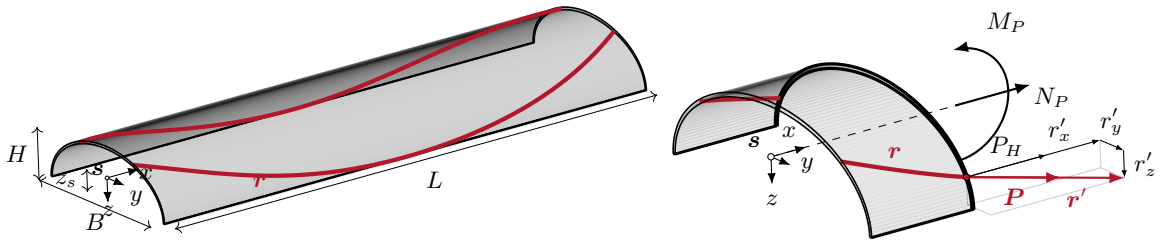

Figure 1: Model of a prestressed spatial beam-like structure and the internal forces due to prestress.

The objective function is $\mathcal{J}_P : \mathbb{R}^3 \rightarrow \mathbb{R}$. The constraints are described by $\boldsymbol{g} : \mathbb{R} \rightarrow \mathbb{R}^3$. The Ritz-polynomial $\tilde{\boldsymbol{r}}$ approximating the tendon layout is defined by its order $n \in \mathbb{R}$ and its coefficients $\boldsymbol{a} \in \mathbb{R}^n$. $M_E : \mathbb{R} \rightarrow \mathbb{R}$ and $M_P : \mathbb{R} \rightarrow \mathbb{R}$ are the moments due to external loads (e) and prestress (p) respectively. M_E depends on the static system, loading and the structure's geometry. M_P depends on the tendon layout and the prestressing force. The functions $f_y : \mathbb{R} \rightarrow \mathbb{R}$ and $f_z : \mathbb{R} \rightarrow \mathbb{R}$ are the components of the surface function $\boldsymbol{S}(u, v) = [u,\ f_y(u, v),\ f_z(u, v)]^T$ and describe the cross-section of the thin-walled concrete structure. The vector function $\boldsymbol{P} : \mathbb{R} \rightarrow \mathbb{R}^3$ describes the prestressing force with magnitude

$$P(x) = |\boldsymbol{P}(x)| \in \mathbb{R} \tag{8}$$

The prestressing force is always directed in the same direction as the tendon.

$$\boldsymbol{P}(x) = P(x) \frac{\boldsymbol{r}'(x)}{|\boldsymbol{r}'(x)|} \tag{9}$$

In this paper, only the moment about the y-axis is considered. It is assumed that the tendons are arranged symmetrically along the y-axis, so that no moment occurs about the z-axis.

$$M_{P,y}(x) = -P_H(x)\ r_z(x) = -P\ \frac{r_z\ r'_x}{\sqrt{r'^2_x + r'^2_y + r'^2_z}} \tag{10}$$

3.1. Consideration of losses during the optimization

As described above the prestressing force in the tendon is reduced by prestress losses. These losses may change along the tendon. Thus, instead of a constant prestressing force as assumed by Domnick and Osman-Letelier [1], it changes along x and depends on loss specific parameters. With the initial prestressing force $\boldsymbol{P}_0$ and the prestress losses $\Delta\boldsymbol{P}$, the prestressing force $\boldsymbol{P}$ is described by

$$\boldsymbol{P}(x) = \boldsymbol{P}_0(x) - \Delta\boldsymbol{P}(x) \tag{11}$$

Assuming the prestressing force is always directed in the direction of the tendon allows for the following transformation

$$|\boldsymbol{P}| \frac{\boldsymbol{r}'}{|\boldsymbol{r}'|} = |\boldsymbol{P}_0| \frac{\boldsymbol{r}'}{|\boldsymbol{r}'|} - |\Delta\boldsymbol{P}| \frac{\boldsymbol{r}'}{|\boldsymbol{r}'|} \Rightarrow |\boldsymbol{P}| = |\boldsymbol{P}_0| - |\Delta\boldsymbol{P}| \tag{12}$$

Thus, it is sufficient to consider its magnitude

$$P(x) = P_0 - \Delta P(x) \tag{13}$$

3.2. Losses due to friction

3.2.1. Calculation of friction losses

Friction losses directly derive from the tendon layout. Consequently, taking these prestress losses into account during the tendon layout optimization has a great benefit for the achieved design as the resulting losses can automatically be counteracted by the tendon layout itself. This is why, in this paper, the effects of friction losses are considered as an example to be included in the optimization process.

$$\Delta P(x) = \Delta P_\mu(x) \tag{14}$$

Combining equations (13) and (14) leads to the following resulting prestressing force in the tendon

$$P(x) = P_0 - \Delta P_\mu(x) \tag{15}$$

The friction between the tendon and the surrounding material depends on the prestressing force P, the angle ϑ and the friction coefficient μ between tendon and surrounding material. Generally, the variation of the force as shown in Figure 2 is described by the following differential equation [3]:

$$\frac{d\,P}{d\,\vartheta} - \mu\,P = 0 \tag{16}$$

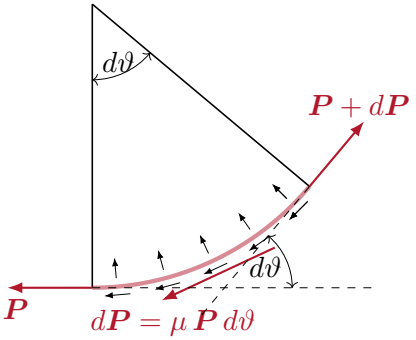

Figure 2: Variation of the prestressing force $\boldsymbol{P}$ due to friction in an infinitesimal element of the tendon.

The general solution of equation (16) is described by the EULER-EYTELWEIN equation [3]:

$$P_{hold} = P_{load}\,e^{-\mu\,\vartheta} \tag{17}$$

Where P_{hold} is the resulting force $P(x)$ under the influence of friction along the tendon and P_{load} is the initial force P_0. The angle $\vartheta(x)$ describes the accumulated angle deviation up to the point x along the tendon.

$$P(x) = P_0\,e^{-\mu\,\vartheta(x)} \tag{18}$$

Combining equations (15) and (18) results in

$$\Delta P(x) = P_0\,\left(1 - e^{-\mu\,\vartheta(x)}\right) \tag{19}$$

Friction losses depend on the layout of jacking and anchoring. In this paper, jacking from one end is assumed. As shown in Figure 3, for jacking from one end the maximum friction losses $\Delta P_{\mu,max}$ equal $P_{jack} - P_{anchor}$, where P_{jack} is the initial prestressing force applied at the jacking. P_{anchor} is the prestressing force at the anchor of the tendon at the other end of the structure.

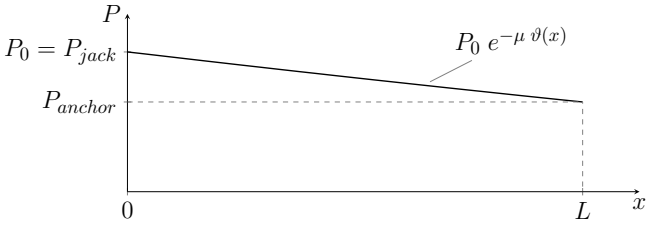

Figure 3: Prestressing force under the influence of friction for jacking from one end.

3.2.2. Calculation of total angle deviation $\vartheta(x)$

In order to determine friction losses, it is necessary to calculate the total angle deviation of the tendon denoted as $\vartheta(x)$, which can be calculated as follows:

$$\vartheta(x) = \theta(x, r) + k\,x \tag{20}$$

In equation (20) $\theta(x, r)$ is the accumulated angle deviation due to the layout of the spatial tendon (intended angle deviation) and k is the wobble coefficient that accounts for unintended angle deviation due to minor deviations from the intended profile. Values for the wobble coefficients are given by the manufacturers for example in the European Technical Assessment (ETA).

The total angle deviation θ along the tendon in the two-dimensional case (tendon lies in the xz-plane) is described by equation (21), as the tendon is only curved with respect to the y-axis. Considering its absolute value accounts for the accumulation of the angle, independent of its sign. Note, that for small angles s can be approximated by x.

$$\theta(s) = \int_{s_0}^{s} \left| \frac{d\theta}{d\tilde{s}} \right| \, d\tilde{s} \tag{21}$$

$$\frac{d\theta}{ds} \approx \frac{d\theta}{dx} = \frac{d}{dx} \frac{d\, r_z}{dx} = \frac{d^2\, r_z}{dx^2} \tag{22}$$

$$\theta(x) = \int_{x_0}^{x} \left| r_z''(\tilde{x}) \right| \, d\tilde{x} \tag{23}$$

In folded slabs as in Figure 4 the spatial tendon lies in a tilted plane. This means it is curved with respect to one axis, i.e. not doubly curved. However, in contrast to the two-dimensional case described above, this is not necessarily a coordinate axis. Therefore, it is not sufficient to consider r_z in order to calculate θ as in equation (23). For folded slabs, the angle θ can be calculated by transforming the tendons coordinate system as follows.

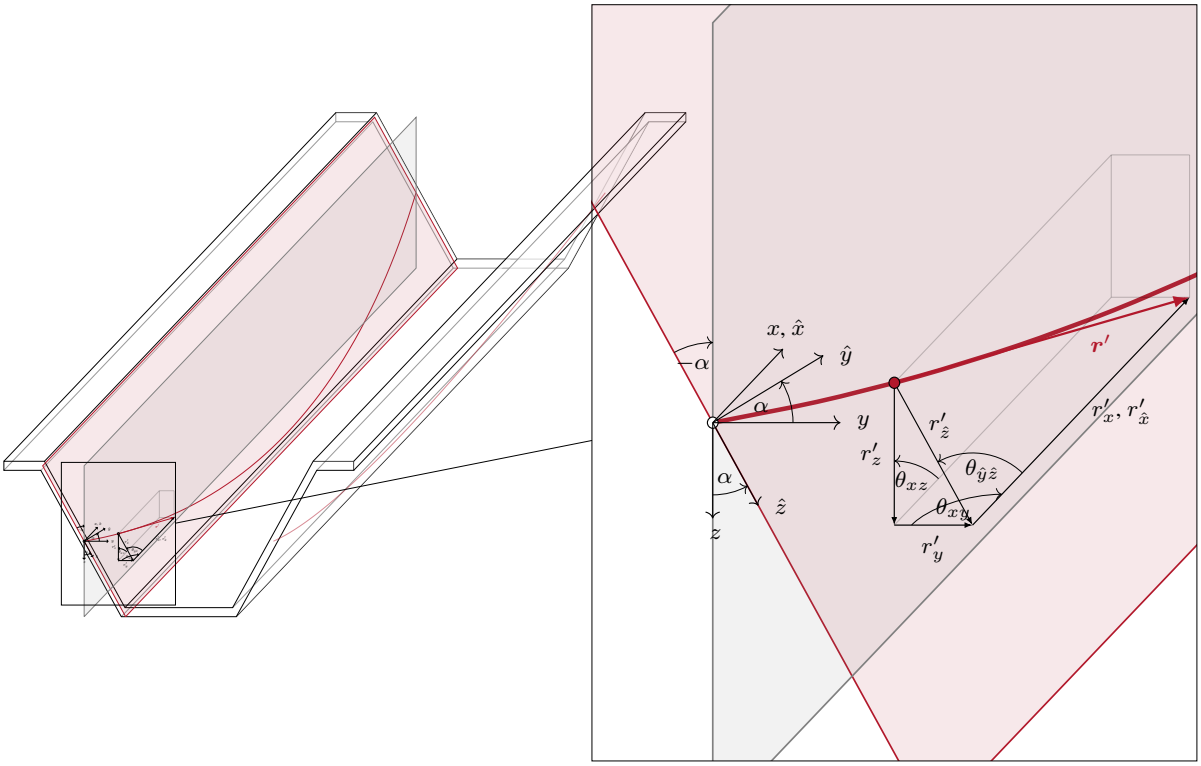

Figure 4: Curvature of a tendon in a folded slab.

Figure 4 shows that in a folded slab the tendon is restricted to the tilted plane defined by the angle α to the xz-plane. As shown by Domnick and Osman-Letelier [1] the tendon is described by

$$\boldsymbol{r}(x) = \begin{bmatrix} r_x \\ r_y \\ r_z \end{bmatrix} = \begin{bmatrix} x \\ -\tan(\alpha)\, r_z \\ r_z \end{bmatrix} \tag{24}$$

For such a tendon a plane with coordinate system $\hat{x}$, $\hat{y}$, $\hat{z}$ exists, so that the coefficient $r_{\hat{y}}$ disappears and the curvature is completely described by the coefficient $r_{\hat{z}}$

$$\hat{\boldsymbol{r}}(x) = \begin{bmatrix} r_{\hat{x}} \\ r_{\hat{y}} \\ r_{\hat{z}} \end{bmatrix} = \begin{bmatrix} r_{\hat{x}} \\ 0 \\ r_{\hat{z}} \end{bmatrix} \tag{25}$$

For a folded slab this plane equals the tilted plane described by the rotation angle α around the x-axis. This means by rotating $\boldsymbol{r}(x)$ with the rotation matrix around the x-axis

$$\mathbf{R}_x(\varphi) = \begin{bmatrix} 1 & 0 & 0 \\ 0 & \cos(\varphi) & -\sin(\varphi) \\ 0 & \sin(\varphi) & \cos(\varphi) \end{bmatrix} \tag{26}$$

by an angle $\varphi = -\alpha$ the form described in equation (25) can be achieved as follows:

$$\hat{\boldsymbol{r}}(x) = \mathbf{R}_x(-\alpha)\, \boldsymbol{r}(x) = \begin{bmatrix} 1 & 0 & 0 \\ 0 & \cos(-\alpha) & -\sin(-\alpha) \\ 0 & \sin(-\alpha) & \cos(-\alpha) \end{bmatrix} \begin{bmatrix} r_x \\ r_y \\ r_z \end{bmatrix} = \begin{bmatrix} r_x \\ \cos(\alpha)\, r_y + \sin(\alpha)\, r_z \\ -\sin(\alpha)\, r_y + \cos(\alpha)\, r_z \end{bmatrix} \tag{27}$$

With

$$r_y = -\tan(\alpha)\, r_z = -\frac{\sin(\alpha)}{\cos(\alpha)} r_z \tag{28}$$

and $\cos(\alpha) = \cos$ and $\sin(\alpha) = \sin$ equation (27) yields

$$\hat{\boldsymbol{r}}(x) = \begin{bmatrix} r_x \\ -\cos\frac{\sin}{\cos}\, r_z + \sin\, r_z \\ -\sin\, r_y + \cos\, r_z \end{bmatrix} = \begin{bmatrix} r_x \\ -\sin\, r_z + \sin\, r_z \\ -\sin\, r_y + \cos\, r_z \end{bmatrix} = \begin{bmatrix} r_x \\ 0 \\ \sqrt{(-\sin\, r_y + \cos\, r_z)^2} \end{bmatrix} \tag{29}$$

$$\begin{aligned} &= \begin{bmatrix} r_x \\ 0 \\ \sqrt{\sin^2 r_y^2 - \sin\cos r_y r_z - \sin\cos r_y r_z + \cos^2 r_z^2} \end{bmatrix} \\ &= \begin{bmatrix} r_x \\ 0 \\ \sqrt{\sin^2 r_y^2 - \left(-\frac{\cos}{\sin}\right)\sin\cos r_y r_y - \left(-\frac{\sin}{\cos}\right)\sin\cos r_z r_z + \cos^2 r_z^2} \end{bmatrix} \\ &= \begin{bmatrix} r_x \\ 0 \\ \sqrt{\sin^2 r_y^2 + \cos^2 r_y^2 + \sin^2 r_z^2 + \cos^2 r_z^2} \end{bmatrix} = \begin{bmatrix} r_x \\ 0 \\ \sqrt{\left(\sin^2 + \cos^2\right)\left(r_y^2 + r_z^2\right)} \end{bmatrix} \\ &= \begin{bmatrix} r_x \\ 0 \\ \sqrt{r_y^2 + r_z^2} \end{bmatrix} \end{aligned} \tag{30}$$

Equation (30) demonstrates that the rotated tendon $\hat{\boldsymbol{r}}(x)$ has no eccentricity to the tilted plane ($r_{\hat{y}} = 0$) and the angle θ is described by the coefficient $r_{\hat{z}}$. Furthermore, $\hat{\boldsymbol{r}}(x)$ has exactly the expected form as stated in equation (25). With $r_x = x$ the accumulated angle deviation is then described by

$$\theta(x) = \theta_{\hat{y}\hat{z}}(x) = \int_{x_0}^{x} \left| \frac{d^2 r_{\hat{z}}(\tilde{x})}{d\tilde{x}^2} \right| d\tilde{x} = \int_{x_0}^{x} \left| r_{\hat{z}}''(\tilde{x}) \right| d\tilde{x} = \int_{x_0}^{x} \left| \left(\sqrt{r_y^2(\tilde{x}) + r_z^2(\tilde{x})} \right)'' \right| d\tilde{x} \tag{31}$$

Combining equations (15), (19), (20) and (31) leads to the following description of the prestressing force along the spatial tendon in a folded slab with consideration of prestress losses due to friction, extending the solution algorithm described by equations (1) to (7).

$$P(x) = P_0 - \Delta P_\mu(x) \tag{32}$$

$$\text{with} \quad \Delta P_\mu(x) = P_0 \left(1 - e^{-\mu\ \vartheta(x)}\right) = P_0 \left(1 - e^{-\mu(\theta(x,r)+k\ x)}\right) \tag{33}$$

$$\text{and} \quad \theta(x,r) = \int_{x_0}^{x} \left| \left(\sqrt{r_y^2(\tilde{x}) + r_z^2(\tilde{x})}\right)'' \right| d\tilde{x} \tag{34}$$

4. Examples

Two examples of tendon layouts in thin-walled concrete structures with the consideration of prestress losses are presented. The results are obtained by implementing the algorithm described in section 3 (equations (1) to (7) and (32) to (34)) in MATLAB (©MathWorks, Version R2023b). The built-in functions *vpaintegral* and *vpasolve* are used to solve the integral in $\mathcal{J}_P$ and the system of equations $\nabla\mathcal{L} = \mathbf{0}$.

For both examples, the following parameters concerning geometry, loading, and degree of the polynomial are defined: $L = 30\ m$, $H = 5\ m$, $k = 0,005$, $g_1 = 3\ \frac{kN}{m}$, $g_2 = 4\ \frac{kN}{m}$, $q = 2\ \frac{kN}{m}$, $n = 16$. A simply supported beam as shown in Figure 5 without geometrical constraints is considered. To fully utilize the vertical space available, an optimal initial prestressing force P_0 is chosen for each example.

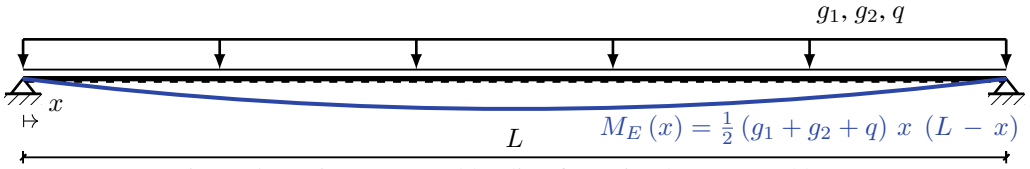

Figure 5: Static system and loading for a simply supported beam.

The effectiveness of the optimized tendon layout is compared to a common alternative design approach: a simplified solution that ignores the gradient of the tendon ($r_i'(x) \approx 0$ for slender beams)

$$\boldsymbol{r}_{simp}(x) = \begin{bmatrix} x \\ f_y(x) \\ M_E(x)/P_0 \end{bmatrix} \tag{35}$$

4.1. Optimization of a planar tendon layout in a T-beam

In a T-beam, as shown in Figure 6, the tendon is located in the xz-plane with $f_y = 0$ and $f_z = v$. With $v = \boldsymbol{a}^T\boldsymbol{\phi}(x)$ this leads to the following approximation for the tendon:

$$\tilde{\boldsymbol{r}}(x) = \begin{bmatrix} u \\ f_y \\ f_z \end{bmatrix} = \begin{bmatrix} u \\ 0 \\ v \end{bmatrix} = \begin{bmatrix} x \\ 0 \\ \boldsymbol{a}^T\boldsymbol{\phi}(x) \end{bmatrix} \tag{36}$$

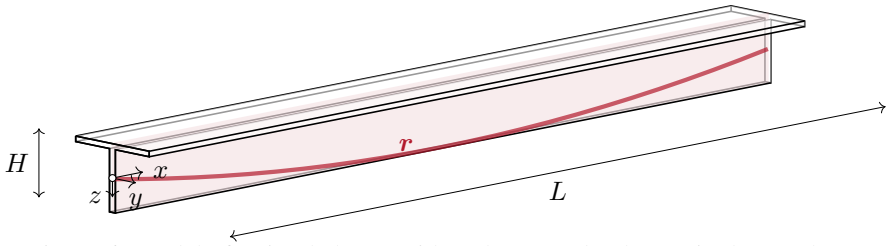

Figure 6: Model of a simple beam with a planar tendon layout in the xz-plane.

Figure 7 shows the optimized tendon layout considering an initial prestressing force of $P_0 = 440\ kN$. The objective function has been minimized to $\mathcal{J}_P = 2,4 \cdot 10^{-6}\ (kN\ m)^2\ m$. The total prestress losses due to friction, as shown in Figure 9, accumulated to $\Delta P_{max}/P_0 = 16\%$ at the right end of the beam.

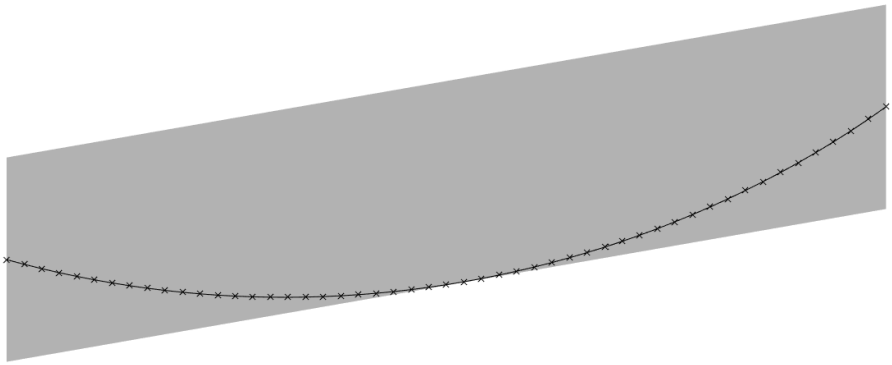

Figure 7: Optimized planar tendon layout in a T-beam.

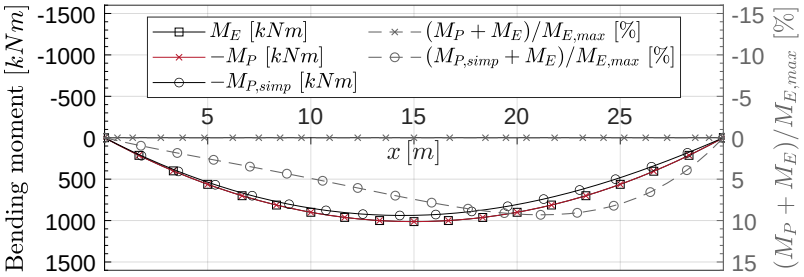

Figure 8: Bending moments due to external loads and prestress.

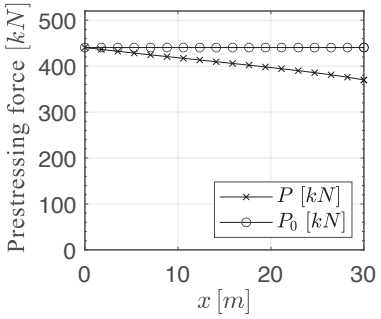

Figure 9: Initial prestressing force P_0 and prestressing force with consideration of friction losses $P(x)$.

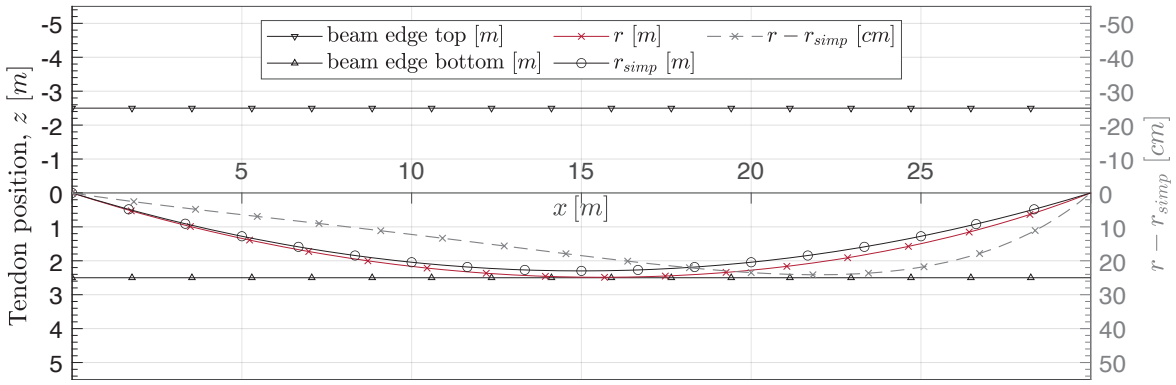

Figure 10: Vertical component r_z of the optimized tendon layout in comparison to the simplified approach according to equation (35).

4.2. Optimization of a spatial tendon layout in a folded slab

The tilted plane of a folded slab, as shown in Figure 11, is described by the functions $f_y = -\tan(\alpha)\ v$ and $f_z = v$. In the example an angle $\alpha = \frac{\pi}{4}$ was chosen. With $v = \boldsymbol{a}^T \boldsymbol{\phi}(x)$ this leads to the following approximation for the tendon:

$$\boldsymbol{r}(x) = \begin{bmatrix} u \\ f_y \\ f_z \end{bmatrix} = \begin{bmatrix} u \\ -\tan(\pi/4)v \\ v \end{bmatrix} = \begin{bmatrix} x \\ -\boldsymbol{a}^T \boldsymbol{\phi}(x) \\ \boldsymbol{a}^T \boldsymbol{\phi}(x) \end{bmatrix} \tag{37}$$

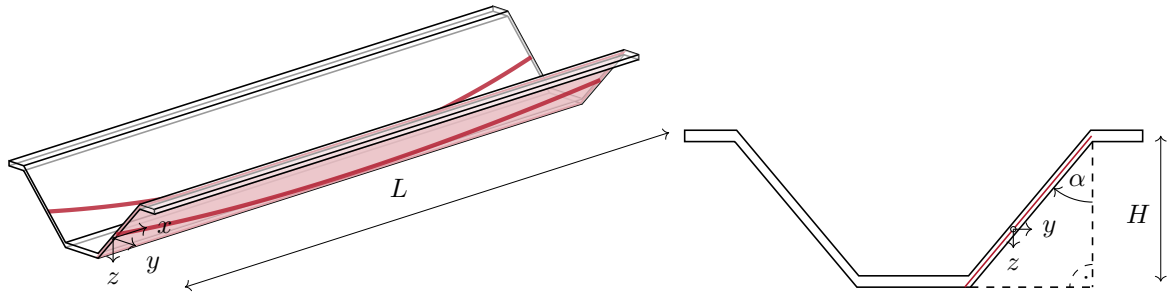

Figure 11: Model of a folded slab with a spatial tendon layout.

Figure 12 shows the optimized tendon layout considering an initial prestressing force of $P_0 = 451\ kN$. The objective function has been minimized to $\mathcal{J}_P\ = 3,4 \cdot 10^{-3}\ (kN\ m)^2\, m$. The total prestress losses due to friction, as shown in Figure 14, accumulated to $\Delta P_{max}/P_0 = 22\%$ at the right end of the beam.

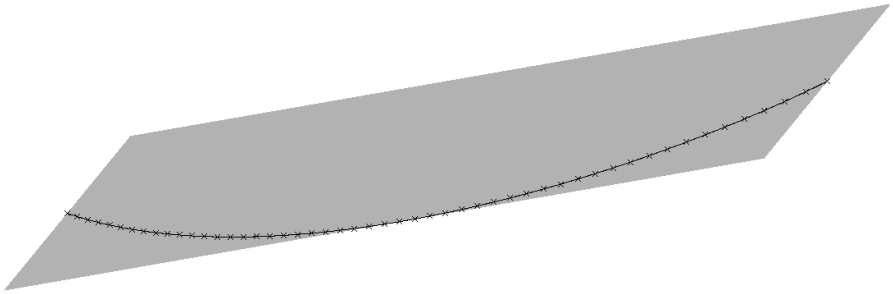

Figure 12: Optimized spatial tendon layout in a folded slab.

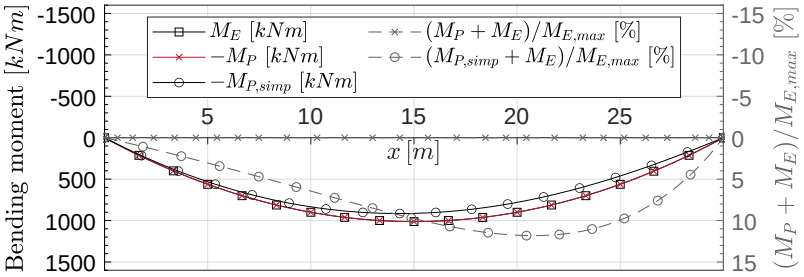

Figure 13: Bending moments due to external loads and prestress.

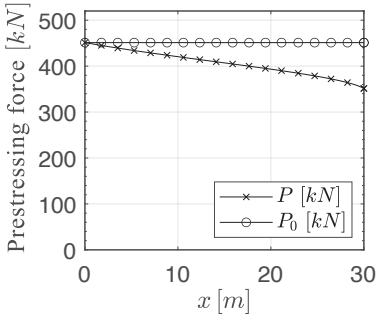

Figure 14: Initial prestressing force P_0 and prestressing force with consideration of friction losses $P(x)$.

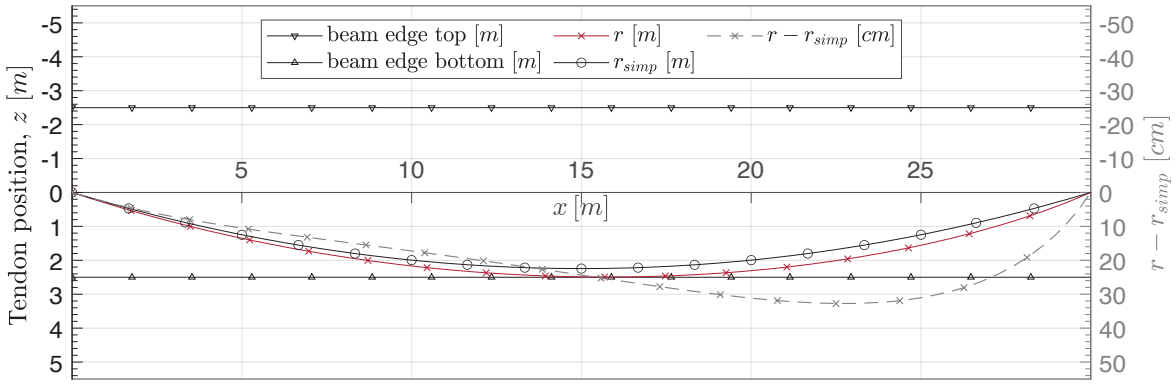

Figure 15: Vertical component r_z of the optimized spatial tendon layout in comparison to the simplified approach according to equation (35).

4.3. Analysis and comparison of the results

The obtained results demonstrate that the optimized tendon is able to fully counteract the friction losses. For both study cases the remaining moment $M_p + M_e$ is reduced to practically 0% of the maximum moment by the optimized tendon layout (see Figures 8 and 13). In comparison, a tendon layout designed with the simplified approach and without considering friction losses results in a remaining moment $M_{p,simp} + M_e$ of up to 9% and 12%. The objective function $\mathcal{J}_P$ as an indicator for the solution's quality was reduced to values of less than $10^{-2}\,(kNm)^2\,m$. The absolute difference between the optimized tendon layout and the simplified approach (see Figures 10 and 15) is about 25 cm for the T-beam and 33 cm for the folded slab. This equals about 10% and 13% of the maximum eccentricity of the tendon.

The structures in both study cases have the same span, height and loading. Solely the additional horizontal eccentricity and curvature of the tendon in the folded slab increased the friction losses by $(22\% - 16\%)/16\% = 37\%$. This shows the high impact of the spatial layout of the tendon, demonstrating the importance of its consideration during the design stage.

5. Conclusion

In this paper, the optimization method for spatial tendon layouts in thin-walled concrete structures, which was successfully applied in the past by Domnick and Osman-Letelier [1] for a constant prestressing force, has been extended to include the consideration of prestress losses. The concept for the consideration of prestress losses in general was shown and the formulation of the optimization method extended accordingly. Friction losses were investigated more in depth as they directly derive from the tendon layout and its curvature. The results of the presented study cases, a two-dimensional tendon layout in a beam and a three-dimensional tendon layout in a folded slab, demonstrate that the optimized tendon layouts are able to fully compensate the loss in prestress by friction losses.

The comprehensive approach presented in this paper provides a more accurate and realistic representation of the structural behavior in prestressed spatial concrete structures and their optimization. Prestress losses reduce the effectiveness of prestress in a structure substantially. By reliably compensating them in the design stage, more robust and efficient structures are possible. Thus, by enhancing the understanding of the associated complexities, the presented approach contributes to advancements in structural engineering and saving material through structural optimization, which is a key component in redefining the art of structural design.

References

[1] H. Domnick and J. P. Osman-Letelier, "Development of 3d mathematical models for tendon layout optimization by strain energy minimization," in *Proceedings of IASS Annual Symposia*, Melbourne, Australia, 2023, pp. 1529–1540.

[2] J. P. Osman-Letelier, "Investigation on structural behaviour of prestressed thin-walled concrete structures," Dissertation, Technical University of Berlin, Berlin, Germany, 2024.

[3] K. Zilch and G. Zehetmaier, *Bemessung im konstruktiven Betonbau: Nach DIN 1045-1 (Fassung 2008) und EN 1992-1-1 (Eurocode 2)*. Heidelberg: Springer-Verlag, 2010.

[4] L. A. Caro, J. R. Marti-Vargas, and P. Serna, "Prestress losses evaluation in prestressed concrete prismatic specimens," *Engineering Structures*, vol. 48, pp. 704–715, 2013.

[5] P. Zia, H. K. Preston, N. L. Scott, and E. B. Workman, "Estimating prestress losses," *Concrete International*, vol. 1, no. 6, pp. 32–38, 1979.

[6] G. de Roeck, "Vorspannungsverluste bei beliebig gekrümmtem spanngliedverlauf," *Beton- Und Stahlbetonbau*, vol. 73, pp. 123–124, 1978.